Bulletin of the Seismological Society of America, Vol. 106, No. 6, pp. 2450–2458, December 2016, doi: 10.1785/0120160100

Ⓔ

Automatic Aftershock Forecasting: A Test Using Real-Time Seismicity Data in Japan

by Takahiro Omi, Yosihiko Ogata, Katsuhiko Shiomi, Bogdan Enescu,* Kaoru Sawazaki, and Kazuyuki Aihara

Abstract Real-time aftershock forecasting is important to reduce seismic risks after a damaging earthquake. The main challenge is to prepare forecasts based on the data available in real time, in which many events, including large ones, are missing and large hypocenter determination errors are present due to the automatic detection process of earthquakes before operator inspection and manual compilation. Despite its practical importance, the forecast skill of aftershocks based on such real-time data is still in a developmental stage. Here, we conduct a forecast test of large inland aftershock sequences in Japan using real-time data from the High Sensitivity Seismograph Network (Hi-net) automatic hypocenter catalog (Hi-net catalog), in which earthquakes are detected and determined automatically in real time. Employing the Omori–Utsu and Gutenberg–Richter models, we find that the proposed probability forecast estimated from the Hi-net catalog outperforms the generic model with fixed parameter values for the standard aftershock activity in Japan. Therefore, the real-time aftershock data from the Hi-net catalog can be effectively used to tailor forecast models to a target aftershock sequence. We also find that the probability forecast based on the Hi-net catalog is comparable in performance to the one based on the latest version of the manually compiled hypocenter catalog of the Japan Meteorological Agency when forecasting large aftershocks with $M > 3.95$, despite the apparent inferiority of the automatically determined Hi-net catalog. These results demonstrate the practical usefulness of our forecasting procedure and the Hi-net automatic catalog for real-time aftershock forecasting in Japan.

Online Material: Figures and tables showing detailed forecast results for all considered aftershock sequences and all forecast time frames.

Introduction

Aftershock forecasting is one of the important scientific responses after a large earthquake. In recent decades, much effort has been taken to develop forecasting methods of aftershocks (e.g., Reasenberg and Jones, 1989; Gerstenberger *et al.*, 2005; Ogata and Katsura, 2006; Hainzl *et al.*, 2009; Woessner *et al.*, 2011; Nanjo *et al.*, 2012; Omi *et al.*, 2013, 2014, 2015; Steacy *et al.*, 2013). Although retrospective forecast tests have examined the predictability of aftershocks, such tests have generally used the best compiled data (revised data) available at the time of respective studies for preparing forecasts, which are not available in real time (Woessner *et al.*, 2011; Nanjo *et al.*, 2012). The data available in real time (real-time data) are inferior in quality compared with the manually compiled data, especially for the early stage of aftershock sequences. In particular, real-time data suffer from missing many aftershocks, including large ones, or from apparent misidentified aftershocks. In addition, real-time data include large epicenter determination errors. Therefore, it is necessary to test forecasting models using real-time data to evaluate their real-time forecast skills (Marzocchi and Lombardi, 2009; Omi *et al.*, 2013; Steacy *et al.*, 2013).

Here we conduct a forecast test for aftershock sequences of the seven inland mainshocks of M 7 class in Japan using the real-time data from the High Sensitivity Seismograph Network (Hi-net) automatic hypocenter catalog by the National Research Institute for Earth Science and Disaster Resilience (NIED; Okada *et al.*, 2004). We first address

*Also at The Institute of Statistical Mathematics, 10-3 Midori-cho, Tachikawa, Tokyo 190-8562, Japan.

whether sequence-specific forecasts based on real-time data are effective. Because the statistical properties of aftershocks are considerably different depending on the analyzed sequence, the forecasts could be improved by employing specific parameter values, tailored to an individual aftershock sequence based on the available data. In fact, by using the revised data, it has been shown that such sequence-specific forecasts outperform generic models equipped with fixed parameter values that represent the standard aftershock activities in the respective target regions (Woessner *et al.*, 2011; Omi *et al.*, 2015). However, it remains unclear whether this is also the case for real-time data. Second, we examine how the forecast performance depends on data quality. We use the revised data from the Japan Meteorological Agency (JMA) unified catalog to compare forecast performances between the Hi-net catalog and the JMA catalog.

Data

In this study, we use two hypocenter catalogs in Japan, the Hi-net automatic catalog (Okada *et al.*, 2004), and the JMA unified catalog. All events in the Hi-net catalog are automatically detected and determined in real time by servers at the NIED. Each event is registered to the catalog about 6–7 min after its occurrence, on average. Once the data are registered, they are not modified later. Therefore, the Hi-net catalog enables us to conduct the forecast test using real-time data.

The JMA unified catalog is compiled based on the waveform data from seismograph networks of the JMA, NIED, and universities and other institutes in Japan. All detected earthquakes in the JMA catalog are manually checked and compiled. As seen in the Incompleteness of the Hi-net Automatic Catalog Relative to the JMA Catalog section, the JMA catalog is superior to the Hi-net catalog, especially for the early part of the aftershock sequences. However, the preliminary JMA catalog is updated only once a day because of the time required to manually inspect and compile the data, and therefore there is a time lag of about one day before the data are available. Furthermore, the preliminary JMA catalog is repeatedly revised over time (e.g., the new events are retrospectively added). In this study, we use the latest version of the JMA catalog as reference data.

In the following, we consider aftershock sequences of the seven inland mainshocks of M 7 class that occurred after the establishment of the Hi-net observation system. Specifically they are the 2000 Western Tottori earthquake of M_J 7.3, the 2004 Chuetsu earthquake of M_J 6.8, the 2005 west off Fukuoka earthquake of M_J 7.0, the 2007 off Chuetsu earthquake of M_J 6.8, the 2007 Noto Peninsula earthquake of M_J 6.9, the 2008 Iwate–Miyagi Nairiku earthquake of M_J 7.2, and the 2014 Northern Nagano earthquake of M_J 6.7, in which M_J is the JMA magnitude.

Here, it should be noted that not all the mainshocks are listed in the Hi-net automatic catalog because the determination of strong-motion earthquakes by the Hi-net is not stable because of its highly sensitive nature (i.e., targeted to record small events). Specifically, the hypocenters of some mainshocks were not properly determined because their seismograms (in particular the large amplitude S waves) were saturated. A bias in picking the S-wave arrival would result in a biased event location. Therefore, when analyzing the Hi-net catalog in this study, we adopt the mainshock information (time, location, and magnitude) from the JMA catalog, which is generally almost the same as the one announced by the JMA very soon after the mainshock occurrence.

Incompleteness of the Hi-net Automatic Catalog Relative to the JMA Catalog

In this section, we examine the incompleteness of the Hi-net automatic catalog relative to the latest version of the manually compiled JMA catalog for the early stage of aftershock sequences.

Spatial Distribution

Figure 1 compares the spatial distribution of the aftershocks in the first day after the 2004 Chuetsu earthquake between the Hi-net and JMA catalogs (see Ⓔ Figs. S1–S7, available in the electronic supplement to this article, for the other aftershock sequences). While the aftershocks in the JMA catalog form a tight cluster around the mainshock, those in the Hi-net catalog are widely scattered far beyond the cluster recorded in the JMA catalog. To quantitatively characterize the spatial distribution, we plot the number of earthquakes inside a square centered at the mainshock as a function of its side length (Fig. 2). For the JMA catalog, almost all aftershocks are confined in a square region with the normalized side length of $d' = 1$ (the dashed line in Fig. 2b; also refer to Fig. 2 caption for details), which corresponds to the Utsu–Seki aftershock zone length, $D(M_0) = 0.01 \times 10^{0.5M_0-1.8}$ degrees, inferred from the mainshock magnitude M_0 (Utsu, 1969), namely ~50 km for $M_0 = 7$ (this square is also shown by a small square of the dashed line in Fig. 1). We regard such a square region as the "standard" aftershock zone. On the other hand, a significant fraction of the aftershocks in the Hi-net catalog is outside this standard aftershock zone (Figs. 1 and 2a). These observations indicate that the Hi-net automatic catalog has large location errors during the early stage of aftershock sequences. The location error may further lead to inaccurate magnitude determination, but we do not deal with this issue in this article.

Considering the large location errors in the Hi-net catalog, we use a relatively large aftershock zone as compared to the standard one to ensure a better catalog completeness; that is, the side length of the aftershock zone is set to $4D(M_0)$, four times the Utsu–Seki aftershock zone length, as shown by a large square of solid line in Figure 1. In the following sections, we analyze the earthquakes in the defined aftershock zones. Although this definition is somewhat *ad hoc*, the results obtained in the following are robust against the change in the

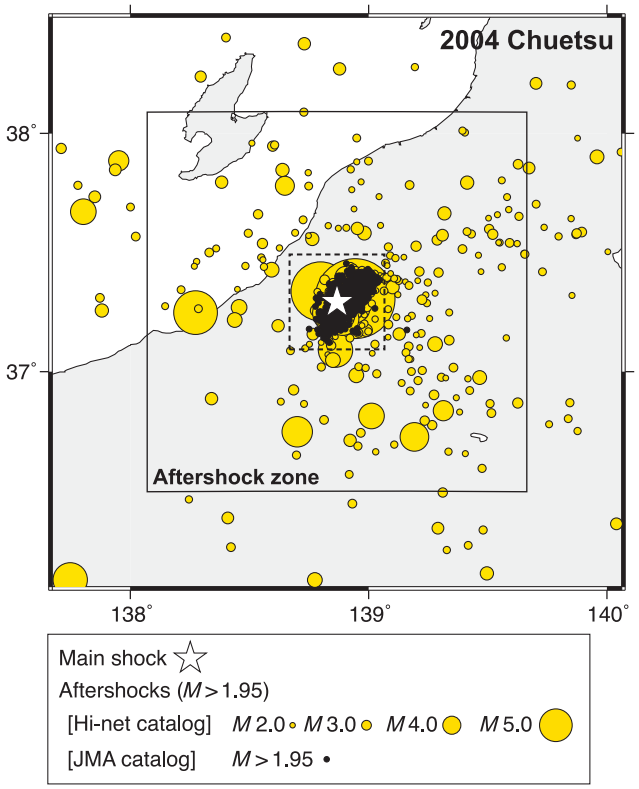

Figure 1. Spatial distribution of earthquakes of $M > 1.95$ in the first 24 hrs of the 2004 M 6.8 Chuetsu earthquake. The dashed small square line of side length $D(M_0)$ inside the panel represents the standard aftershock zone, in which $D(M_0)$ is the Utsu–Seki aftershock zone length, $D(M_0) = 0.01 \times 10^{0.5M_0-1.8}$ degrees, inferred from the mainshock magnitude M_0. The solid larger square line of side length $4D(M_0)$ inside the panel represents an aftershock zone used in this study. The color version of this figure is available only in the electronic edition.

aftershock zone size. To be sure, we checked this for cases with the side lengths of $3D(M_0)$ and $5D(M_0)$.

Magnitude Frequency

It is well known that early small aftershocks are systematically missing from seismic catalogs due to overlapping seismic waves from the mainshock and the following frequent aftershocks, which makes real-time forecasting particularly difficult (Utsu *et al.*, 1995; Kagan, 2004; Enescu *et al.*, 2009; Peng and Zhao, 2009; Sawazaki and Enescu, 2014). Although data incompleteness is observed in both the Hi-net and JMA catalogs, the Hi-net catalog is clearly more deficient than the JMA catalog, especially during the first few hours after the mainshock (Fig. 3; also see Ⓔ Figs. S1–S7 for the other aftershock sequences). Furthermore, some large aftershocks, such as those with $M > 3.95$, are also missing in the Hi-net catalog during this period. Therefore, the real-time data from the Hi-net automatic catalog is substantially more incomplete than the revised data from the JMA catalog during the early stage. The aftershock detection ability of the Hi-net system gradually recovers with time. In fact, the magnitude–frequency distributions of the Hi-net and JMA catalogs are similar during the 12–24 hr period after the mainshock in the 2004 Chuetsu aftershock sequence (Fig. 3e).

Forecasting Experiment

Settings

In this study, we focus on short-term forecasts based on the early part of an aftershock sequence in which the difference between the real-time and revised data is prominent. Specifically, our test consists of four time frames, which use the first 3, 6, 12, and 24 hr periods of aftershock data to prepare forecasts for the following 3, 6, 12, and 24 hr periods, respectively. For each time frame, we forecast the number of aftershocks in magnitude bins of the width of 0.1 magnitude unit over the range $M_t < M < 8.05$, in which M_t is a target magnitude and the last bin contains the earthquakes with $M > 8.05$. We consider two target magnitudes, $M_t = M_c$ and $M_t = 3.95$, in which M_c is the completeness threshold magnitude in each forecast period for each sequence. Each value of the completeness magnitude M_c is listed in Ⓔ Table S1.

We only briefly describe the forecast models used in this study (see Appendix A for details). We prepare and compare three different forecasts based on the Omori–Utsu law that describes the aftershock frequency versus time from the mainshock (Omori, 1894; Utsu, 1961; Utsu *et al.*, 1995) and the Gutenberg–Richter law for the magnitude–frequency distribution of earthquakes (Gutenberg and Richter, 1944). The first and second forecasts are sequence specific: we estimate the parameter values from the aftershock data in a learning period based on the Hi-net and JMA catalogs, respectively. The third forecast uses the fixed parameter values (the generic model) determined based on many aftershock sequences in Japan (see Appendixes A and C). The forecast from the generic model depends only on the mainshock magnitude. Each forecast is then evaluated based on the actual observation recorded in the JMA catalog and quantified by the log-likelihood score. The performance of competitive forecasts is measured by the log-likelihood ratio score (Appendix A and Helmstetter *et al.*, 2006), which is referred to as information gain in this study.

To determine the parameter values of the sequence-specific forecasts from the early aftershock data, we statistically characterize the data incompleteness using the detection rate function of the elapsed time and magnitude of an aftershock (Ogata and Katsura, 2006; Omi *et al.*, 2013). By combining the detection rate function with the above-mentioned forecast model, we can estimate the parameter values directly from the incomplete data. We also consider the estimation uncertainty of the parameter values (Akaike, 1978; Nomura *et al.*, 2011; Omi *et al.*, 2015). If we estimate the parameter values from the early aftershock data, the estimation often has a large uncertainty. In such cases, the forecasting can often be

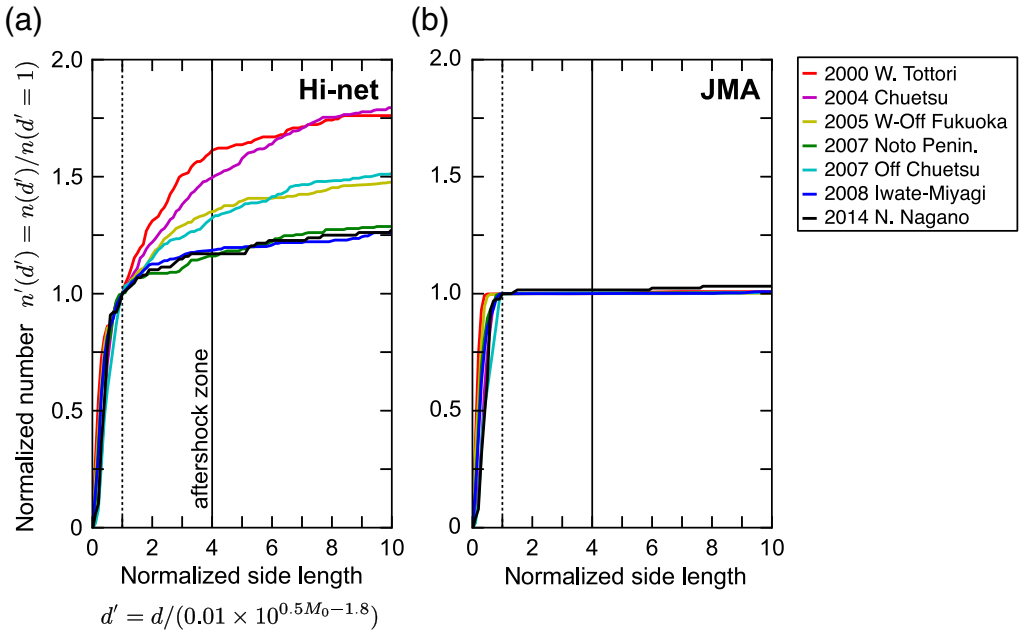

Figure 2. The number of earthquakes of $M > 1.95$ in the first 24 hrs within the square centered at the mainshock is plotted as a function of its side length d for (a) the High Sensitivity Seismograph Network (Hi-net) and (b) the Japan Meteorological Agency (JMA) catalogs. The side length d is normalized by the empirical aftershock zone length as $d' = d/D(M_0)$, in which $D(M_0) = 0.01 \times 10^{0.5M_0-1.8}$ degrees for the mainshock magnitude M_0. The number is also normalized so that the normalized number becomes 1 at $d' = 1$. The vertical lines at $d' = 1$ (dashed) and 4 (solid) respectively correspond to the standard aftershock zone and the one employed in this study. The color version of this figure is available only in the electronic edition.

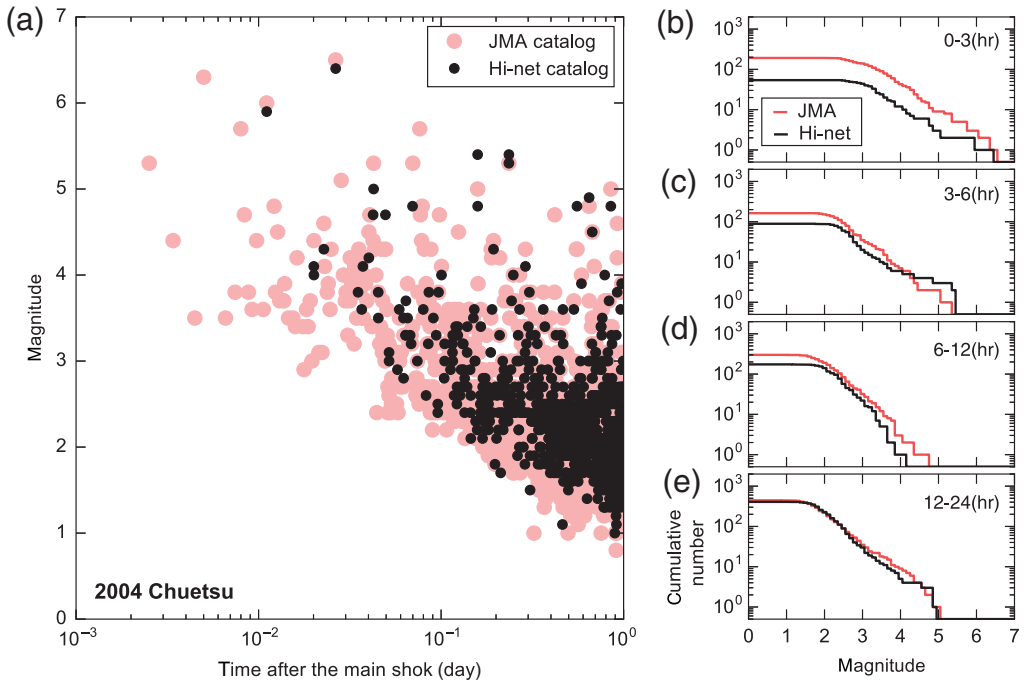

Figure 3. Plots of magnitude versus time in a logarithmic scale and the empirical cumulative magnitude distribution of the 2004 Chuetsu aftershock sequences from the Hi-net and JMA catalogs. The color version of this figure is available only in the electronic edition.

severely biased if we only use a single parameter set for the forecasting (plug-in forecasting). Alternatively, we combine the forecasts from many likely parameter samples to obtain more robust forecasts (Bayesian forecasting). In our previous study, we found that Bayesian forecasting outperforms plug-in forecasting (Omi *et al.*, 2015). Therefore, throughout the present study, we adopt Bayesian forecasting except for the generic model in which the parameters are fixed.

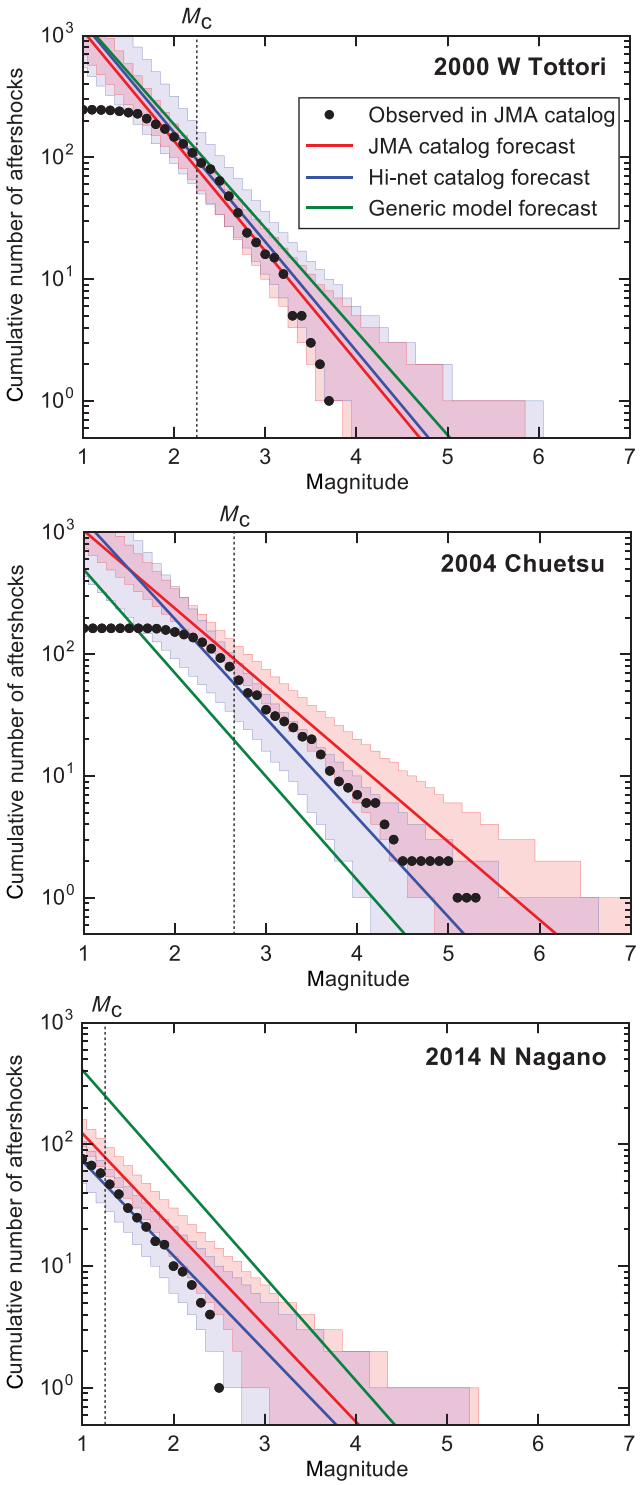

Figure 4. Examples of aftershock forecasts for the 2000 Western Tottori earthquake, the 2004 Chuetsu earthquake, and the 2014 Northern Nagano earthquake for the forecast period 3–6 hrs after the mainshock. In each panel, the solid lines represent the forecasted numbers of aftershocks (see the legend for details). A shaded region represents the 95% interval predicted on the basis of each aftershock data. The dots are the empirical cumulative number of detected aftershocks for the 3–6 hr period (JMA catalog). The color version of this figure is available only in the electronic edition.

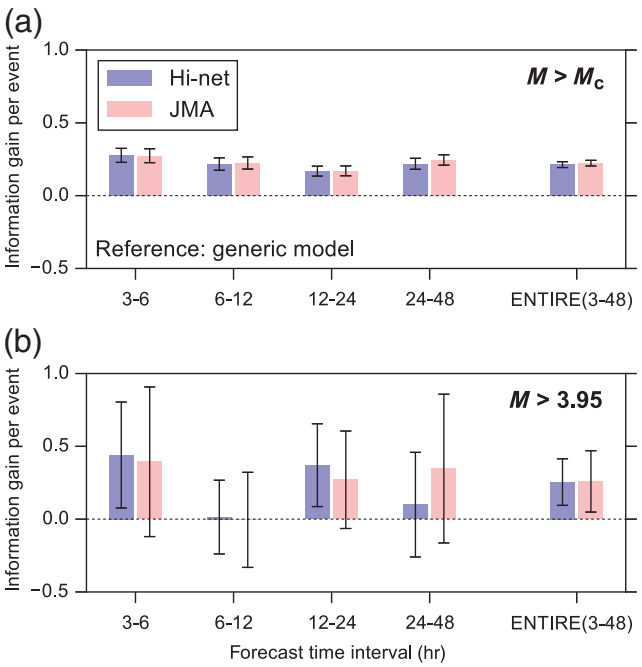

Figure 5. Information gain per aftershock of the forecasts respectively based on the Hi-net and JMA catalogs relative to the generic model for the cases with (a) $M > M_c$ and (b) $M > 3.95$. If the lower bound of the error bar is greater than 0, the forecast is significantly better than the generic model with $p > 95\%$ (see Appendix A for details). The color version of this figure is available only in the electronic edition.

Results

Figure 4 shows the forecast results for the 3–6 hr period for three aftershock sequences (see Ⓔ Figs. S1–S7 for the other sequences and other time frames). The generic model is sometimes consistent with the observations, such as for the 2000 Western Tottori aftershock sequence; however, it clearly overestimates or underestimates the observation for the other cases, such as the 2004 Chuetsu and 2014 Northern Nagano aftershock sequences (Fig. 4). This is because the generic model uses the fixed parameter values and cannot adapt to individual aftershock sequences. On the other hand, the sequence-specific forecasts, tailored by using the available data, are more consistent with the observations as compared to the generic model (Fig. 4). Therefore, the sequence-specific forecast is useful for aftershock forecasting.

Figure 5 shows the information gain per aftershock of the two individual sequence-specific forecasts based respectively on the Hi-net and JMA catalogs against the generic aftershock model over the seven examined aftershock sequences, which measures the individual forecast accuracy relative to the generic model (Ⓔ see Tables S1–S2 for the score of each sequence and each time frame). A forecast is significantly better than the generic model with $p > 95\%$, if the lower bound of the error bar in Figure 5 is greater than 0 (see Appendix A for details). For the entire forecast period of 3–48 hrs, both the Hi-net and JMA forecasts significantly outperform the generic

model, which demonstrates that the sequence-specific forecast is effective even for the automatically determined real-time data in providing quick and more accurate estimations of aftershock rates after large inland earthquakes. In addition, the same result is valid in all individual forecast periods for the case of the lowest target magnitude $M_t = M_c$, as shown in Figure 5a. On the other hand, for the case of the high target magnitude $M_t = 3.95$, the scores of the sequence-specific forecasts are generally better than that of the generic model in individual forecast periods, but this is not statistically significant for most cases, as shown in Figure 5b. The scores tend to have large error bars for the high target magnitude because of a small number of large aftershocks in the seven considered aftershock sequences.

Finally, we compare the forecast performances between the Hi-net automatic catalog and the JMA revised catalog to examine the dependence of performance on data quality. The information gain per aftershock for the JMA forecast over the Hi-net forecast for the entire forecast period (3–48 hrs) is 0.010 ± 0.002 and 0.005 ± 0.051 for the low and high target magnitudes, respectively. Thus, the JMA forecast significantly outperforms the Hi-net forecast in the case of the small target magnitude $M_t = M_c$. This is natural because the early aftershock data from the JMA catalog are clearly superior to those in the Hi-net catalog, as seen in Figure 3. On the other hand, it is fortunate to know that the performance of the Hi-net forecast is comparable to that of the JMA forecast for the large aftershocks, despite the relative incompleteness of the real-time data. In forecasting large aftershocks, which are small in number, the Bayesian forecasting performances may be insensitive against the fine choice of the parameter values (Omi *et al.*, 2015). This result demonstrates the usefulness of the Hi-net automatic catalog in real-time forecasting of large aftershocks.

Conclusions and Discussion

In this article, we demonstrated the feasibility of operational real-time aftershock forecasts directly using automatically detected aftershock data. We conducted a forecast test for aftershock sequences of the seven inland earthquakes of M 7 class in Japan using the Hi-net automatic hypocenter catalog. First, we found that the forecast based on the Hi-net catalog performs significantly better than the generic model. This indicates that the sequence-specific forecast is effective with the incomplete real-time data even though the real-time automatic data are inferior to the manually revised data, especially for the early stage of aftershocks of the M 7 class mainshocks. It is noted that the parameters in the generic model is determined based on the JMA catalog. Second, we demonstrated that the forecasts based on the Hi-net catalog and the latest compiled version of the JMA catalog are comparable in performance for forecasts of large aftershocks of $M > 3.95$. This indicates that the Hi-net automatic catalog is useful for real-time aftershock forecasting in Japan.

Only a few forecast experiments using real-time data have been conducted so far despite its practical importance (Marzocchi and Lombardi, 2009; Omi *et al.*, 2013; Steacy *et al.*, 2013). One reason for this is that at present the real-time data are not usually available, because the hypocenter catalogs are, in general, continuously updated, and the revised ones overwrite the initial ones. Fortunately, the Hi-net automatic catalog has kept and provides the real-time earthquake data in Japan, which enabled us to carry out this retrospective forecast test with the real-time data. To encourage the testing of forecasts based on the real-time data, it would be helpful if the seismological institutions worldwide archive their real-time data. Because in Japan both data and methodology are available, our study would pave the way for the next generation of real-time prospective aftershock forecasting in Japan.

Data and Resources

The High Sensitivity Seismograph Network (Hi-net) automatic catalog is provided by the National Research Institute for Earth Science and Disaster Resilience (NIED), which is not available to the public. Registered users can download the real-time hypocenter data of earthquakes in the latest two days from the NIED Hi-net website (https://hinetwww11.bosai.go.jp/auth/hinet_hypolist/?LANG=en), although this list in the website is not exactly the same as the Hi-net automatic catalog (e.g., this list is sometimes manually modified). The Japan Meteorological Agency (JMA) unified catalog is available at the JMA website (http://www.data.jma.go.jp/svd/eqev/data/bulletin/hypo_e.html, last accessed January 2016).

Acknowledgments

We would like to thank the Japan Meteorological Agency (JMA), the National Research Institute for Earth Science and Disaster Resilience (NIED), and universities for providing the data. The JMA unified catalog used in this study is produced by the JMA, in cooperation with the Ministry of Education, Culture, Sports, Science and Technology. T. O. is supported by the Japan Society for the Promotion of Science (JSPS) fellowship for young scientists postdoctoral fellow. T. O., Y. O., and B. E. are also supported by JSPS KAKENHI Grant 26240004. K. A. is supported by CREST, Japan Science and Technology Agency.

References

Akaike, H. (1978). A new look at the Bayes procedure, *Biometrika* **65,** 53–59.

Akaike, H. (1980). Likelihood and the Bayes procedure, in *Bayesian Statistics*, J. M. Bernardo, M. H. DeGroot, D. V. Lindley, and A. F. M. Smith (Editors), University Press, Valencia, Spain, 143–166 (discussion 185–203).

Enescu, B., J. Mori, M. Miyazawa, and Y. Kano (2009). Omori–Utsu law c-values associated with recent moderate earthquakes in Japan, *Bull. Seismol. Soc. Am.* **99,** 884–891, doi: 10.1785/0120080211.

Gerstenberger, M. C., S. Wiemer, L. M. Jones, and P. A. Reasenberg (2005). Real-time forecasts of tomorrow's earthquakes in California, *Nature* **435,** 328–331.

Gutenberg, B., and C. F. Richter (1944). Frequency of earthquakes in California, *Bull. Seismol. Soc. Am.* **34,** 185–188.

Hainzl, S., B. Enescu, M. Cocco, J. Woessner, F. Catalli, R. Wang, and F. Roth (2009). Aftershock modeling based on uncertain stress calculations, *J. Geophys. Res.* **114,** no. B05309, doi: 10.1029/2008JB006011.

Helmstetter, A., Y. Y. Kagan, and D. D. Jackson (2006). Comparison of short-term and time-independent earthquake forecast models for southern California, *Bull. Seismol. Soc. Am.* **96,** 90–106.

Iwata, T. (2008). Low detection capability of global earthquakes after the occurrence of large earthquakes: Investigation of the Harvard CMT catalogue, *Geophys. J. Int.* **174,** 849–856.

Jackson, D. D., and Y. Y. Kagan (1999). Testable earthquake forecasts for 1999, *Seismol. Res. Lett.* **70,** 393–403.

Kagan, Y. Y. (2004). Short-term properties of earthquake catalogs and models of earthquake source, *Bull. Seismol. Soc. Am.* **94,** 1207–1228.

Kass, R. E., and A. E. Raftery (1995). Bayes factors, *J. Am. Stat. Assoc.* **90,** 773–795.

Marzocchi, W., and A. M. Lombardi (2009). Real-time forecasting following a damaging earthquake, *Geophys. Res. Lett.* **36,** L21302, doi: 10.1029/2009GL040233.

Marzocchi, W., J. D. Zechar, and T. H. Jordan (2012). Bayesian forecast evaluation and ensemble earthquake forecasting, *Bull. Seismol. Soc. Am.* **102,** 2574–2584.

Nanjo, K. Z., H. Tsuruoka, S. Yokoi, Y. Ogata, G. Falcone, N. Hirata, Y. Ishigaki, T. H. Jordan, K. Kasahara, K. Obara, *et al.* (2012). Predictability study on the aftershock sequence following the 2011 Tohoku-Oki, Japan, earthquake: First results, *Geophys. J. Int.* **191,** 653–658.

Nomura, S., Y. Ogata, F. Komaki, and S. Toda (2011). Bayesian forecasting of recurrent earthquakes and predictive performance for a small sample size, *J. Geophys. Res.* **116,** no. B04315, doi: 10.1029/2010JB007917.

Ogata, Y., and K. Katsura (1993). Analysis of temporal and spatial heterogeneity of magnitude frequency distribution inferred from earthquake catalogues, *Geophys. J. Int.* **113,** 727–738.

Ogata, Y., and K. Katsura (2006). Immediate and updated forecasting of aftershock hazard, *Geophys. Res. Lett.* **33,** L10305, doi: 10.1029/2006GL025888.

Okada, Y., K. Kasahara, S. Hori, K. Obara, S. Sekiguchi, H. Fujiwara, and A. Yamamoto (2004). Recent progress of seismic observation networks in Japan—Hi-net, F-net, K-NET and KiK-net, *Earth Planets Space* **56,** 15–28.

Omi, T., Y. Ogata, Y. Hirata, and K. Aihara (2013). Forecasting large aftershocks within one day after the main shock, *Sci. Rep.* **3,** 2218.

Omi, T., Y. Ogata, Y. Hirata, and K. Aihara (2014). Estimating the ETAS model from an early aftershock sequence, *Geophys. Res. Lett.* **41,** 850–857, doi: 10.1002/2013GL058958.

Omi, T., Y. Ogata, Y. Hirata, and K. Aihara (2015). Intermediate-term forecasting of aftershocks from an early aftershock sequence: Bayesian and ensemble forecasting approaches, *J. Geophys. Res.* **120,** 2561–2578, doi: 10.1002/2014JB011456.

Omori, F. (1894). On the aftershocks of earthquake, *J. Coll. Sci. Imp. Univ. Tokyo* **7,** 111–200.

Peng, Z., and P. Zhao (2009). Migration of early aftershocks following the 2004 Parkfield earthquake, *Nat. Geosci.* **2,** 877–881.

Reasenberg, P. A., and L. M. Jones (1989). Earthquake hazard after a mainshock in California, *Science* **243,** 1173–1176.

Ringdal, F. (1975). On the estimation of seismic detection thresholds, *Bull. Seismol. Soc. Am.* **65,** 1631–1642.

Sawazaki, K., and B. Enescu (2014). Imaging the high-frequency energy radiation process of a main shock and its early aftershock sequence: The case of the 2008 Iwate-Miyagi Nairiku earthquake, Japan, *J. Geophys. Res.* **119,** 4729–4746, doi: 10.1002/2013JB010539.

Steacy, S., M. Gerstenberger, C. Williams, D. Rhoades, and A. Christphersen (2013). A new hybrid Coulomb/statistical model for forecasting aftershock rates, *Geophys. J. Int.* **196,** 918–923.

Utsu, T. (1961). A statistical study on the occurrence of aftershocks, *Geophys. Mag.* **30,** 521–605.

Utsu, T. (1969). Aftershocks and earthquake statistics (1): Some parameters which characterize an aftershock sequence and their interrelations, *J. Fac. Sci., Hokkaido Univ., Ser. VII (Geophysics)* **3,** 129–195.

Utsu, T., Y. Ogata, and R. S. Matsu'ura (1995). The centenary of the Omori formula for a decay law of aftershock activity, *J. Phys. Earth* **43,** 1–33.

Woessner, J., S. Hainzl, W. Marzocchi, M. J. Werner, A. M. Lombardi, F. Catalli, B. Enescu, M. Cocco, M. C. Gerstenberger, and S. Wiemer (2011). A retrospective comparative forecast test on the 1992 Landers sequence, *J. Geophys. Res.* **116,** no. B05305, doi: 10.1029/2010JB007846.

Appendix A

Detailed Method for the Forecast and Evaluation

Our forecast model is based on our previous studies (Omi *et al.*, 2013, 2014, 2015). We employ a model of the occurrence rate of underlying aftershocks of magnitude M at elapsed time t from the mainshock, given as

$$\lambda(t, M) = \frac{K}{(t+c)^p} \beta e^{-\beta(M-M_0)}. \tag{A1}$$

Here, the parameters K, c, and p from the Omori–Utsu (O-U) formula for aftershock decay and the parameter β from the Gutenberg–Richter (G-R) formula for the magnitude–frequency relation ($\beta = b \ln 10$) are constants to be estimated, and M_0 represents the mainshock magnitude.

For a while after the mainshock, many small aftershocks are missing from the seismic catalogs. To statistically characterize this data incompleteness, we employ the detection rate of an aftershock of magnitude M at an elapsed time t after the mainshock, given as

$$\Phi(M|\mu(t), \sigma) = \frac{1}{\sqrt{2\pi\sigma^2}} \int_{-\infty}^{M} dx \exp\left[-\frac{(x-\mu(t))^2}{2\sigma^2}\right]. \tag{A2}$$

The detection rate is modeled by the cumulative normal distribution (the error function) of the magnitude M at each time t (Ringdal, 1975; Ogata and Katsura, 1993; Iwata, 2008). Here, the 50% detection magnitude $\mu(t)$ varies in time, and the parameter σ represents the range of the magnitude of partially detected earthquakes. The introduction of the detection rate enables us to make use of all the available data including the earthquakes below the completeness threshold magnitude. To make the following estimation plausible, we assume the form $\mu(t) = \mu_0(t) + \mu_1$ and fix the time-varying part $\mu_0(t)$ to the one estimated by the Bayesian smoothing method (Akaike, 1980) proposed in our previous studies (Omi *et al.*, 2013, 2014, 2015). Therefore, the time-varying parameter $\mu(t)$ can be reduced to a single parameter μ_1.

For the sequence-specific forecasts using the hypocenter catalog, the parameter set $\theta = (K, p, c, \beta, \mu_1, \sigma)$ of the forecasting model in equation (A1) and the detection rate function in equation (A2) is estimated in the following Bayesian framework. The posterior probability distribution posterior$(\theta|\mathbf{X}^{[0,S]}_{\text{learn}})$

of the parameter set θ given the data $\mathbf{X}_{\text{learn}}^{[0,S]}$ in the learning period $[0, S]$ after the mainshock is obtained from Bayes' theorem as follows:

$$\text{posterior}(\theta|\mathbf{X}_{\text{learn}}^{[0,S]}) \propto \tilde{L}(\theta|\mathbf{X}_{\text{learn}}^{[0,S]}) \times \text{prior}(\theta), \tag{A3}$$

in which $\tilde{L}(\theta|\mathbf{X}_{\text{learn}}^{[0,S]})$ and $\text{prior}(\theta)$ are a likelihood function and a prior probability distribution, respectively, which are given in Appendix B.

We adopt a Bayesian forecasting approach (Akaike, 1978) to prepare robust forecasts from short-term data after the mainshock. In this approach, we use many parameter sets $\{\theta_i\}$ sampled from the posterior probability distribution in equation (A3) by using the Markov chain Monte Carlo simulation method and combine the forecasts from these parameter sets (Omi *et al.*, 2015).

In this article, our forecast takes the form of a predictive distribution $P^{[S,T]}(\{n_j\})$ of the numbers $\{n_j\}$ of aftershocks with magnitudes $\{M_j\}$ above a target magnitude M_t in a forecasting period $[S, T]$. Given a parameter set θ_i, the predictive probability distribution $P^{[S,T]}(n_j|\theta_i)$ of the number n_j of aftershocks with magnitude M_j in the forecasting period $[S, T]$ is obtained by the Poisson distribution with the mean given as

$$\int_S^T dt \int_{M_j-0.05}^{M_j+0.05} dM\lambda(t, M|\theta_i). \tag{A4}$$

Therefore, the full predictive distribution $P^{[S,T]}(\{n_j\}|\theta_i)$ for a parameter set θ_i is given by

$$P^{[S,T]}(\{n_j\}|\theta_i) = \prod_{M_j>M_t} P^{[S,T]}(n_j|\theta_i). \tag{A5}$$

The predictive distribution $P^{[S,T]}(\{n_j\}|\{\theta_i\})$ of the Bayesian forecasting is obtained by averaging the predictive distribution $P^{[S,T]}(\{n_j\}|\theta_i)$ from each parameter set θ_i over the parameter sets $\{\theta_i\}$, that is,

$$P^{[S,T]}(\{n_j\}|\{\theta_i\}) = \sum_{i=1}^{N} P^{[S,T]}(\{n_j\}|\theta_i)/N, \tag{A6}$$

in which N is the number of parameter sets; for example, $N = 1000$ in our study.

For the generic model, the predictive distribution is given by equation (A5). Its parameter values are set to $\beta = 1.96$, $K = 7.75 \times 10^{-3}$, $p = 1.05$, and $c = 1.80 \times 10^{-2}$ (day) (see Appendix C for details).

Given the observed numbers $\{n_j^*\}$ of aftershocks with magnitudes above the target magnitude in the forecasting period, each forecasting performance is quantified by the log-likelihood score $\ln P^{[S,T]}(\{n_j^*\})$. Here, we introduce the information gain of the forecasting model A to model B to compare the performances of the two competing forecasts, which is defined as

$$\text{IG}^{[S,T]}(A, B) = \ln P_A^{[S,T]}(\{n_j^*\}) - \ln P_B^{[S,T]}(\{n_j^*\}). \tag{A7}$$

The information gain is also closely related to the Bayes factor, which is the exponential of the information gain (Kass and Raftery, 1995; Marzocchi *et al.*, 2012). The standard error $\text{ste}^{[S,T]}(A, B)$ of the information gain is numerically obtained as the standard deviation of the information gains over 1000 synthetic data sets $\{n_j\}_k^{Syn}(k = 1, 2, \ldots, 1000)$, which are respectively sampled from the Poisson distribution with the mean set to the observed numbers $\{n_j^*\}$.

To summarize the forecasting performances over all aftershock sequences, we use the information gain per earthquake $\text{IGPE}^{[S,T]}(A, B)$ for a particular forecast period $[S, T]$ and the information gain per earthquake $\text{IGPE}(A, B)$ for the entire forecast period. They are defined as follows:

$$\text{IGPE}^{[S,T]}(A, B) = \sum_S \text{IG}_S^{[S,T]}(A, B)/\sum_S n_S^{[S,T]}, \tag{A8}$$

$$\text{IGPE}(A, B) = \sum_i \sum_S \text{IG}_S^{[S_i,T_i]}(A, B)/\sum_i \sum_S n_S^{[S_i,T_i]}, \tag{A9}$$

in which the subscripts i and s specify a forecast period and an aftershock sequence, respectively, and $n_s^{[T,S]}$ is the number of aftershocks above the target magnitude M_t in the time interval $[T, S]$ for an aftershock sequence s. Their standard errors are given as

$$\text{STE}^{[S,T]}(A, B) = \left[\sum_S \text{ste}_S^{[S,T]}(A, B)^2\right]^{1/2}/\sum_S n_S^{[S,T]}, \tag{A10}$$

$$\text{STE}(A, B) = \left[\sum_i \sum_S \text{ste}_S^{[S_i,T_i]}(A, B)^2\right]^{1/2}/\sum_i \sum_S n_S^{[S_i,T_i]}. \tag{A11}$$

If we assume a simple Gaussian approximation, forecast A is better than forecast B with $p > 95\%$ if we have $\text{IGPE}(A, B) > 1.64 \times \text{STE}(A, B)$.

Although we use the Poisson distribution in estimating the standard error of the information gain in equation (A7), it is known that the earthquake number distribution is more dispersed than the Poisson distribution due to earthquake clustering (Jackson and Kagan, 1999; Omi *et al.*, 2015). Therefore, it is, in general, necessary to consider such non-Poissonian features to appropriately evaluate the confidence interval. However, the secondary or higher-order clusers are not so conspicuous during the early stage of aftershocks, masked by the intense aftershock activity and the lowered detection rate (Omi *et al.*, 2014). Thus, the Poisson distribution could give a reasonable evaluation in our case.

Appendix B

Log-Likelihood Function for the Incomplete Aftershock Data and Prior Function

From the underlying occurrence rate $\lambda(t, M|K, p, c)$ in equation (A1) and the detection rate $\Phi(M|\mu(t), \sigma)$ in equation (A2), the observed occurrence rate $\nu_\theta(t, M)$ is obtained as

$$\nu_\theta(t, M) = \lambda(t, M|K, p, c)\Phi(M|\mu(t), \sigma). \tag{B1}$$

Therefore, the log-likelihood function for the incomplete aftershock data is given by

$$\ln \tilde{L}(\theta|\mathbf{X}_{\text{learn}}^{[0,S]}) = \sum_{\{0<t_i<S\}} \ln \nu_\theta(t_i, M_i) - \int_0^S dt \int_{-\infty}^{+\infty} dM \nu_\theta(t, M). \tag{B2}$$

We note that this method uses all the detected aftershock data including those below the level of the completeness magnitude.

We use mutually independent priors for the p, c, β, and σ parameters in such a way that $\text{prior}(\theta) = \text{prior}(p) \times \text{prior}(c) \times \text{prior}(\beta) \times \text{prior}(\sigma)$. Here, the respective prior is given by $N(1.05, 0.13^2)$, $LN(-4.02, 1.42^2)$, $N(1.96, 0.34^2)$, and $LN(-1.61, 1.0^2)$, in which N denotes the normal distribution and LN denotes the lognormal distribution. These parameters are selected according to Appendix C, except for the *ad hoc* choice of $\text{prior}(\sigma)$ for computational stability; however the results are robust against the variation in $\text{prior}(\sigma)$.

Appendix C

Standard Parameter Values for Aftershock Activity in Japan

To set the priors and the generic parameter values, we fit the Omori–Utsu and Gutenberg–Richter models to 38 aftershock sequences in Japan from the Japan Meteorological Agency (JMA) catalog that were analyzed in Omi *et al.* (2015). The mean and standard deviation of the estimated parameters in equation (A1) are respectively given as $\ln(K) = -4.86 \pm 1.60$, $p = 1.05 \pm 0.13$, $\ln(c[\text{day}]) = -4.02 \pm 1.42$, and $\beta = 1.96 \pm 0.34$.

Institute of Industrial Science
The University of Tokyo
4-6-1 Komaba, Meguro-ku
Tokyo 153-8505, Japan
omi@sat.t.u-tokyo.ac.jp
aihara@sat.t.u-tokyo.ac.jp
(T.O., K.A.)

The Institute of Statistical Mathematics
10-3 Midori-cho, Tachikawa
Tokyo 190-8562, Japan
ogata@ism.ac.jp
(Y.O.)

National Research Institute for Earth Science and Disaster Resilience
3-1 Tennodai, Tsukuba
Ibaraki 305-0006, Japan
shiomi@bosai.go.jp
sawa@bosai.go.jp
(K.S., K.S.)

Department of Geophysics
Graduate School of Science
Kyoto University
Kitashirakawa, Oiwake-cho, Sakyo-ku
Kyoto 606-8502, Japan
benescu@kugi.kyoto-u.ac.jp
(B.E.)

Manuscript received 25 March 2016;
Published Online 20 September 2016